Electrical Power and Energy Systems 121 (2020) 106137

Contents lists available at ScienceDirect

Electrical Power and Energy Systems

journal homepage: www.elsevier.com/locate/ijepes

Optimal design of an adaptive under-frequency load shedding scheme in smart grids considering operational uncertainties

Ali Rafinia, Navid Rezaei*, Jamal Moshtagh

Department of Electrical Engineering, University of Kurdistan, Sanandaj, Iran

ARTICLE INFO

Keywords:
Adaptive under-frequency load shedding
Operational uncertainty
Smart grid
Advanced metering infrastructure
Demand response

ABSTRACT

In the light of the smart grid paradigm, power systems have recently brought about higher levels of adaptability and flexibility. The associated functions in energy management system blocks need to adopt robust strategies to provide greater levels of control and protective service. Under-frequency load shedding (UFLS) schemes can be regarded as a critical function, through which the system integrity and sustainability indices are protected reliably. Conventional UFLS schemes usually suffer from low adaptability and optimal setting in response to changes in the operational characteristics of the power system. This paper seeks to propose an hourly framework for the optimal design of an adaptive UFLS function based on advanced metering infrastructure (AMI) in smart grids. In this portfolio, the target is tailored to fit the main UFLS settings based on the system contingencies and associated operational uncertainties. The simulations are executed on the IEEE 39-bus test system, implemented on a 24-hour scheduling time horizon. The effectiveness of the proposed adaptive model is evaluated with a thorough analysis of the derived numerical results.

1. Introduction

Nowadays, smart grids are becoming a reliable replacement for associated traditional power systems to meet the growing needs of future grids for sustainability, security, and power quality in a more economic and environmental framework. These grids exploit advanced measurement, communication, protection, and control technologies for different parts of the power system [1].

Advanced metering infrastructure (AMI) can be regarded as the fundamental component of the smart grid paradigm. The AMI can measure electrical energy characteristics by establishing two-way telecommunication and provide real-time content processing [2].

Under-Frequency Load Shedding (UFLS) has been designed to optimally shed excessive load corresponding to the active power imbalances and protect the power system against probable frequency collapse risks [3]. The conventional strategies adopted to set the UFLS parameters suffer from a serious drawback. These strategies are not adaptable to the changes in the operational characteristics of the system [4,5]. Adaptive UFLS schemes continuously measure the main quantities of the power system such as frequency, ROCOF, voltage, and active power, and execute the minimum load shedding according to the conditions of the power system after frequency disturbances [6,7]. These schemes rely on fast telecommunication equipment to send load shedding signals to the relays to shed excessive load at maximum speed. Therefore, adaptive UFLS schemes have a suitable performance for both mild and severe contingencies [8].

Nowadays, due to the increase in electricity demand in the smart grid and the destructive environmental impacts of fossil fuels, the tendency of the electricity industry to use renewable energy sources (RESs) has increased worldwide [9]. These sources have replaced some of the conventional generating units. Therefore, the equivalent inertia constant and the active power reserve are reduced, and the frequency control is challenged [10]. With the development of demand response (DR) in the smart grid, some of the loads can respond to frequency variations. The use of DR is vital to improve system frequency response [11].

Plenty of research has focused so far on the strategies of adaptive and conventional UFLS in the smart grid. The main purposes of these studies are to optimize the objective function and minimize the total amount of load shedding given different system constraints. He et al. [12] have developed an adaptive decentralized UFLS method based on load information. Here, a calculation strategy has been achieved using load information resulting from the disturbance to identify the load equivalent virtual inertia in real-time. Then, the optimal adaptive UFLS scheme has been obtained by estimating the load to be shed. In [13] a multistage semi-adaptive UFLS method has been implemented using the

* Corresponding author at: Department of Electrical Engineering, Faculty of Engineering, University of Kurdistan, Kurdistan Province, Sanandaj, Iran.
E-mail address: n.rezaei@uok.ac.ir (N. Rezaei).

https://doi.org/10.1016/j.ijepes.2020.106137
Received 19 February 2020; Received in revised form 3 April 2020; Accepted 19 April 2020

Nomenclature

A. Indices

i	generation units
sc	scenario
s	stage of load shedding
b	under-frequency threshold of generators specified by manufacturer
n	time step of discrete simulation

B. Parameters

f_0	nominal frequency
H_i	inertia time constant of unit i
R_i	governor droop of unit i
S_i	power base of unit i
S	system power base
f_b	threshold of generators under-frequency specified by manufacturer
π^{sc}	probability of scenario sc

C. Continuous variables

$\Delta G^{sc,h}$	generation deficiency due to scenario sc at hour h
$\Delta f_n^{sc,h}$	frequency deviation from nominal value due to scenario sc at time step n and hour h
$\Delta R_n^{sc,h}$	primary frequency regulation due to scenario sc at time step n and hour h
f_s^h	set-point of frequency at stage of load shedding s and hour h
Δdl_s^h	load shedding amount at stage of load shedding s and hour h
Δt_s^h	time delay of under-frequency relay at stage of load shedding s and hour h
$\Delta t_{s,n}^{sc,h}$	time delay of under-frequency relay below set-point f_s^h due to scenario sc at time step n and hour h
$\Delta t_{b,n}^{sc,h}$	time delay of under-frequency relay below the threshold f_b due to scenario sc at time step n and hour h
$\Delta P_w^{sc,h}$	wind power variations due to scenario sc at hour h
$\Delta P_{pv}^{sc,h}$	solar power variations due to scenario sc at hour h
$\Delta P_{lf}^{sc,h}$	load fluctuations duo to scenario sc at hour h

D. Binary variables

$X_{s,n}^{sc,h}$	one, if $\Delta f_n^{sc,h} \; < f_s^h$ due to scenario sc at time step n and hour h, otherwise zero.
$Y_{s,n}^{sc,h}$	one, if $\Delta t_{s,n}^{sc,h} \; > \; \Delta t_s^h$ and $f \; < \; f_s^h$ due to scenario sc at time step n and hour h, otherwise zero.
$Z_{s,n}^{sc,h}$	one, if $f \; < \; f_b$ due to scenario sc at time step n and hour h, otherwise zero.

E. Abbreviations

UFLS	Under-Frequency Load Shedding
ELNS	Expected Load Not Served
MCS	Monte-Carlo Simulation
MILP	Mixed-Integer Linear Programming
PDF	Probability Distribution Function
PV	Photovoltaic
RWM	Roulette Wheel Mechanism

rate of change of frequency (ROCOF). This plan has activated the predetermined last stage as the early stage considering the most severe contingency. Accordingly, islanding and generation scenarios as the most probable power imbalance scenarios are considered in the MILP formulation for the setting of the under-frequency relay. Shekari et al. [14] utilized a centralized adaptive UFLS scheme to obtain an optimal load shedding in three-stage. In the first stage, the requirements for the implementation of this scheme has been presented. In the second stage, considering voltage stability criteria, operational constraints, and interruption cost of the load to be shed, the desired size and location of load and the strategy of load shedding has been specified. In the third stage, the minimum load shedding plan is accomplished with the type of event in real-time. Atighechi et al. [15], expanded a fast UFLS based on a remedial action scheme (RAS). Then, by introducing an efficiency index corresponding to the contribution of each generator and taking into account the dynamics of wind generation, the minimum load shedding is obtained. In [16], a UFLS-MILP scheme to shed the minimum load has been planned by modeling the uncertainties related to system parameters using MCS. Then, by optimal setting the parameters of the ROCOF relay, the power system protects against the islanding caused by frequency drop due to generation deficiency. Darebaghi and Amraee [17] have suggested an innovative probabilistic UFLS strategy to optimize the amount of load to be shed using MILP. Here, the uncertainties using the 3-PEM method are modeled and the obtained results have been compared to the Monte-Carlo Simulation (MCS). Zhenglong et al. [18] introduced a scheme for the optimal setting of the under-frequency relay in the regional power system. In this paper, the multi-generator frequency response (IMFR) model including various governors, spinning reserve, and load has been achieved for the accurate measurement of frequency after the generation-load imbalance. In [19] a novel UFLS scheme based on minimum system prediction frequency has been presented. Here, by sampling the frequency after the contingency, each sample has predicted the minimum system frequency based on the Particle Swarm Optimization (PSO) algorithm. In [20], a UFLS strategy based on the Mixed-Integer Linear Programming (MILP) formulation is introduced with regard to damping and inertia constants. In this method, the amount of load shedding is minimized by taking into account the contingency of the generating units and thus the system frequency drop is avoided. Alagoz *et al.* [21] have proposed a closed-loop PID controller-based price strategy. This study discusses the applicability of optimal energy pricing for control of the energy market to achieve energy balance in case of demand and generation uncertainties. Alagoz and Kaygusuz [22] have suggested online application of smart meters and AC frequency monitoring for control of the energy market to maintain energy balance in case of demand fluctuations. Here, the dynamic energy price is regulated by a closed-loop fractional-order PI control system. The authors analyze energy market management and the performance of this strategy in a multisource energy market model.

Based on a review of the literature, although conventional UFLS has a simpler implementation than adaptive methods, adaptive UFLS sheds less load. Adaptive UFLS on a fast telecommunication platform sheds the optimal amount of load. The prospect of this research is that given our knowledge of the previous works, there is no comprehensive method available for the adaptive setting of the UFLS parameters in which all the uncertainties and conditions of the system are considered. Hence, the purpose of this paper is to set the under-frequency relay parameters considering all system conditions over a 24-hour time horizon in an advanced smart grid.

The contributions and scope of the paper can be highlighted as follows.

- **Optimal load shedding according to hourly conditions in the smart grid.** In this paper, an adaptive strategy is proposed to

improve the performance of the protection system in the smart grid environment. The under-frequency relay parameters can be set at each hour of a day-ahead for reinforcement of the adaptive property. Here, the system parameters such as frequency, equivalent inertia constant, and ROCOF value are measured in real-time. Therefore, the minimum load at each hour is separately shed according to the conditions of that hour on an advanced telecommunication platform in the smart grid.

- **Modeling the uncertainty of generation deficiency, RES power, and load fluctuations.** The hourly changes in generation deficiency, RES power, and load fluctuations are tracked as uncertainty. Given this information in real-time, the three parameters load shedding block, set-point frequency, and time delay for under-frequency relay are separately set over a 24-hour time horizon using the MILP formulation and CPLEX solver. Hence, the above uncertainties are included in the optimal setting of these parameters.
- **Application of DR through an AMI.** Advanced measurement, control, and monitoring technologies for the application of adaptive UFLS are considered in the smart grid. Given the impact of DR on system frequency, the presence of this term is examined in the design of an hourly adaptive UFLS system. Thus, the AMI can measure the active power of load at the consumption side in real-time and thereby determine the amount of DR at each hour.

The rest of the paper is organized as follows. The proposed adaptive UFLS model is described in Section 2. In Section 3, the simulation results of the proposed method are introduced. Finally, the conclusions are drawn in Section 4.

2. Model description

In this paper, an hourly adaptive UFLS strategy is proposed in a smart grid environment. Fig. 1 presents the concept of UFLS in the smart grid considering three platforms, including generation transmission, Supervisory Control And Data Acquisition (SCADA), and consumer section. Power system quantities are measured in real-time by Phasor Measurement Unit (PMU). Simultaneously, the operations of measurement, collection, and analysis of energy consumption are performed by AMI on the demand side. The SCADA unit then monitors and controls the data obtained from these units. The PMU, SCADA, and AMI communicate with each other through a telecommunication system such as a satellite, optical fibers, and the Internet [23]. Whenever under-frequency conditions occur, UFLS relays located at distribution or transmission stations send a load shedding command to the circuit breaker based on the obtained information. In different UFLS schemes, ROCOF is often used in addition to frequency as a quantity for adaptive UFLS schemes. Fig. 2 depicts a typical frequency versus ROCOF curve during under-frequency conditions before and after load shedding. According to this figure, system frequency and ROCOF are 60 Hz and zero, respectively, in the steady-state. After the imbalance of power,

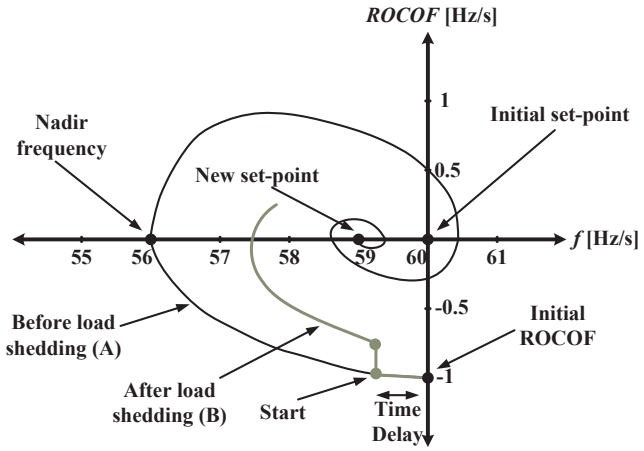

Fig. 2. A typical frequency versus ROCOF curve during under frequency conditions, before and after load shedding.

frequency has a nominal value at the first moment, while ROCOF reaches a non-zero value (Curve A). To balance generation and consumption, the primary frequency regulation by the governor increases active power. Finally, the frequency drops to the lowest value (Nadir frequency) as active power is balanced. When the new steady state is achieved, system frequency is reset to a value below the nominal value as active power increases due to the activation of the primary frequency regulation. To reset frequency to near-nominal frequency, the UFLS strategy must be used. In this case, the frequency drop is low, and the frequency-versus-ROCOF curve (Curve B) is smaller than Curve A [24].

Here, the formulation of the proposed adaptive UFLS scheme is represented in two phases. In the first phase, the process of scenario generation is performed given the uncertainties and different conditions of the system at each hour. In the second phase, the adaptive relay parameters in the stochastic space are optimized using the MILP formulation. In the proposed adaptive UFLS method, therefore, the amount of load shedding is minimized over a 24-hour time horizon.

2.1. Phase-One: Scenario generation and reduction process

In the present paper, the uncertainties associated with generation deficiency due to contingency, wind and solar generation, and load fluctuations for the adaptive setting of under-frequency relay are considered in stochastic space. For the generation of the relevant scenarios, the Probability Distribution Function (PDF) to the forecast error for each uncertainty is obtained with proper accuracy. Weibull function, which is a function of wind speed in the system, is usually considered to describe the probability distribution of wind generation. Although this function represents the random nature of wind generation, however, with a suitable approximation, the Gaussian (normal) distribution

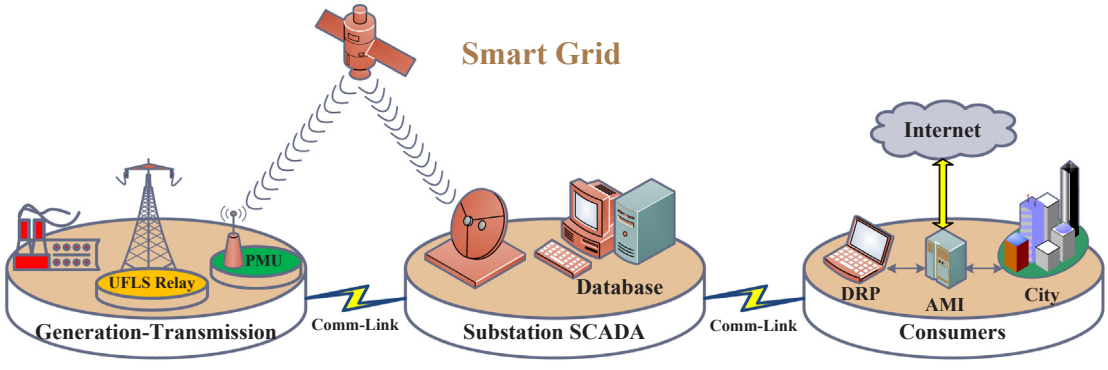

Fig. 1. Adaptive UFLS concept representation in smart grid.

function is considered for modeling the uncertain behavior of both wind and solar generation.

In Fig. 3, the normal PDF and Roulette Wheel Mechanism (RWM) are shown related to the forecast error. In this figure, the continuous curve has been divided into several discrete intervals with standard deviation error (σ) with respect to the zero error mean (μ) in the center of the curve. Each discrete interval has a specific probability (Q). The width of each interval is equal to the standard deviation of the forecast error related to the different uncertainties. It should be noted that uncertainties affect electricity prices, social welfare, and system security and reliability. Hence, the Monte Carlo Simulation (MCS) has been utilized to model the uncertainties based on various forecast levels and probabilities obtained from the proposed PDF to generate the scenario of each hour. Therefore, the probabilities related to each forecast level using RWM are first normalized, that in this case, their sum is 1. In the following, according to Fig. 3, the range between 0 and 1 has been filled by the normalized probabilities and random numbers have been divided between this limit. Each random number falls within the normalized probability range related to the forecast level of the roulette wheel. Therefore, each forecast level has been selected by the RWM as a scenario. The scenario generation procedure has been iterated until the relevant scenarios have been generated. A stopping criterion has been obtained based on the mean value (μ_f) and standard deviation (σ_f) of the forecast parameters. This criterion is expressed by Eq. (1) [25]:

$$cv_f = \frac{\sigma_f}{\mu_f \sqrt{M}} \tag{1}$$

Here, M depicts the number of generated scenarios.

Naturally, as scenarios increase, many uncertainties are covered. In contrast, the complexity of the problem and the volume of computation increase. Therefore, low probable scenarios will increase the problem-solving time. To overcome this problem, the elimination of the least probable and very similar scenarios is performed by the scenario reduction algorithm. This scenario reduction does not change the integrity of the method and provides a good approximation of the uncertainty behavior of the system [26].

Experiences of power system operators show that when a unit has tripped at a given hour, it is not available for all the remaining 24 h. To that end, the scenarios are generated based on the adaptive scenario generation algorithm. Thus, initially, the M scenario is randomly generated for the first hour. Then, the n_{sc} scenario is selected from the most probable scenarios by the scenario reduction algorithm. Selected scenarios in the previous hour are used to generate the scenario in the next hour. The participation of scenarios in the generation of next-hour scenarios yields a better result. To achieve this goal, the probability of each scenario must be calculated from the first hour to a specified hour. For the next hour, the number of scenarios generated by a given scenario is determined by Eq. (2) [27]:

$$n_{h,sc} = Round\left(\frac{\pi_{h-1,sc}}{\sum_{sc=1}^{n_{sc}} \pi_{h-1,sc}} \times M\right) \tag{2}$$

Here $n_{h.sc}$ represents the number of scenarios that are generated at hour h from the scth scenario. $\pi_{h,sc}$ represents the normalized probability of scenario sc from the hour of 1 to h and obtained according to Eq. (3).

$$\pi_{sc} = \frac{\prod_{h=1}^{24}((\sum_{g=1}^{7}\rho_{g,h,sc}^{G}\theta_{g,h})(\sum_{w=1}^{7}\rho_{w,h,sc}^{W}\theta_{w,h})(\sum_{pv=1}^{7}\rho_{pv,h,sc}^{PV}\theta_{pv,h}) (\sum_{l=1}^{7}\rho_{l,h,sc}^{L}\theta_{l,h})\prod_{i=1}^{24}\tau_{i,h,sc}^{GEN})}{\sum_{s=1}^{n_{sc}}\prod_{h=1}^{24}((\sum_{g=1}^{7}\rho_{g,h,sc}^{G}\theta_{g,h})(\sum_{w=1}^{7}\rho_{w,h,sc}^{W}\theta_{w,h}) (\sum_{pv=1}^{7}\rho_{pv,h,sc}^{PV}\theta_{pv,h})(\sum_{l=1}^{7}\rho_{l,h,sc}^{L}\theta_{l,h})\prod_{i=1}^{24}\tau_{i,h,sc}^{GEN}))} \tag{3}$$

Where binary variables $\rho_{g,h,sc}^{G}$, $\rho_{w,h,sc}^{W}$, $\rho_{pv,h,sc}^{PV}$ and $\rho_{l,h,sc}^{L}$ illustrate the status of the selection of gth generation deficiency resulting from contingency interval, wth wind generation interval, pvth solar power generation interval and lth load fluctuations interval at hour h and scenario sc, respectively. If each of these variables accepts the value of 1, the corresponding interval in the roulette wheel is selected. $\theta_{g,h}$, $\theta_{w,h}$, $\theta_{pv,h}$, and $\theta_{l,h}$ according to Fig. 3, represent the probabilities corresponding to the discrete intervals of gth, wth, pvth, and lth at hour h, respectively. $\tau_{i,h,sc}^{GEN}$, returns the share of ith generator in the probability of scenario sc at hour h. If each generator trips at hour h, then for the remaining hours $\tau_{i,h,sc}^{GEN} = 1$.

2.2. Phase-two: Mathematical formulation of the proposed adaptive UFLS strategy

Here, firstly, a discrete-time frequency response has been proposed for modeling the system frequency behavior versus time. Then, the setting of proposed adaptive UFLS system parameters has been characterized based on the MILP formulation in detail.

2.2.1. Discrete-time frequency response model considering power system dynamics

In power systems, the imbalance between generation and consumption causes system frequency deviation. Depending on the governor droop and the inertia constant of the generator, the frequency response of each generator is unique. Therefore, all generators of the power system swing with the common frequency f, simultaneously. $\Delta P_{lm} = D\Delta f$ represents the dependence of the power consumption of motor loads to the frequency. Where D and Δf depict the damping constant and the frequency deviation from nominal value due to the contingency, respectively [28].

The synchronous generators are also equipped with speed governors in power systems. As the frequency changes, the speed governor modifies the active power generation to compensate for the changes. Therefore, the primary frequency regulation is performed using the generator speed governor and is indicated by ΔR. The relation between the active power of the generating unit and the frequency response of the system is shown by the swing equation. Therefore, the frequency response of the system is written as Eq. (4) through an equivalent single-machine swing equation considering the load sensitivity to the frequency changes and the primary frequency regulation of speed governor [28].

$$\frac{d\Delta f(t)}{dt} = \frac{f_0}{2H}(\Delta R(t) - \Delta G + \Delta dl(t) - D\Delta f(t)) \tag{4}$$

Here, $H = \sum_i \frac{H_i S_i}{S}$ depicts the equivalent inertia constant and the base power S; ΔG indicates the amount of generation deficiency; $\Delta dl(t)$ refers to the amount of load shedding at time t. Besides, $\Delta R(t)$ is the primary frequency regulation at time t with governor action, time constant T and the equivalent governor droop $\frac{1}{R} = \sum_i \frac{S_i}{R_i S}$ which is represented by Eq. (5):

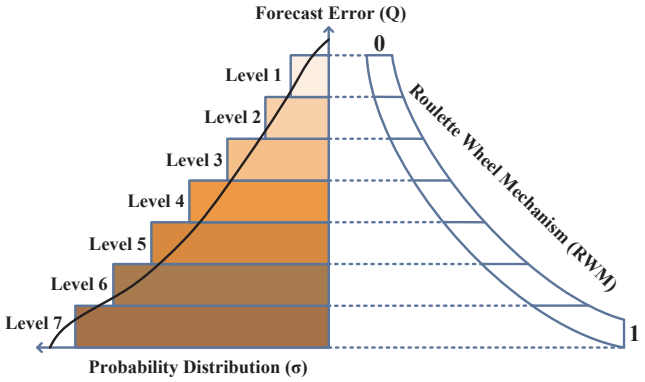

Fig. 3. PDF and RWM related to the forecast error [26].

$$\frac{d\Delta R(t)}{dt} = \frac{1}{T}\left(-\Delta R(t) - \frac{\Delta f(t)}{R}\right) \tag{5}$$

Eqs. (4) and (5) have been discretized into time step Δt by Eq. (6):

$$\begin{cases} \Delta f(n\Delta t) = \Delta f_n \\ \Delta dl(n\Delta t) = \Delta dl_n \\ \Delta R(n\Delta t) = \Delta R_n \end{cases} \tag{6}$$

Then, by Euler's method, Eq. (4) has been converted into discrete form Eqs. (7) and (8).

$$\Delta f_n = \Delta f_{n-1} + RCF_{n-1}\Delta t \tag{7}$$

$$RCF_n = \frac{f_0}{2H}(\Delta R_n - \Delta G + \Delta dl_n - D\Delta f_n) \tag{8}$$

Furthermore, Eq. (5) in discrete form has been transferred into Eq. (9).

$$\Delta R_n = \Delta R_{n-1} \times \left(1 - \frac{\Delta t}{T}\right) - \frac{\Delta t}{T} \times \frac{\Delta f_n}{R} \tag{9}$$

Since there is no frequency deviation or primary frequency regulation before the contingency, it is assumed that the initial conditions of Eqs. (7) and (9) are zero.

2.2.2. MILP formulation for setting of proposed adaptive UFLS strategy

The under-frequency relays at each station detect the under-frequency conditions and thereby shed some of the loads to prevent system frequency instability. Therefore, in these relays, whenever the frequency drops below a certain threshold f, the relay timer is turned on. If the timer exceeds a certain value Δt, the under-frequency relay sends a trip command to shed the load Δdl to the circuit breaker, otherwise, the relay timer is reset. The parameters of the proposed adaptive UFLS system in stochastic space are set using an MILP formulation to minimize the objective function. Three parameter sets at each hour h are considered as the MILP decision variables for the adaptive setting of the under-frequency relay:

(1) frequency set-points, f_s^h
(2) time delay, Δt_s^h
(3) load shedding block, Δdl_s^h

The adaptive UFLS problem presented in this paper contains many variables and complex constraints. Due to the hourly setting of the under-frequency relay parameters, the complexity of the problem multiplies. Therefore, due to the extreme difficulty of the problem, heuristic and trial-and-error methods are unable to find a feasible solution. The adaptive setting of under-frequency relay parameters at each hour of the day-ahead based on the MILP formulation protects the power system against all scenarios with different probability of occurrence. Here, following Eq. (10), a proper objective function has been suggested to minimize the amount of load shedding.

$$OF = \min_{f_s^h,\,\Delta t_s^h,\,\Delta dl_s^h}\left\{\sum_{sc}\left(\pi^{sc}\sum_{s}\Delta dl_s^h\right)\right\} \tag{10}$$

In this scheme, the load block Δdl_s^h has been shed at hour h for the load shedding stage s. If the relay is not hourly set, h is eliminated from the objective function Eq. (10). The objective function in this situation is expressed as Eq. (11).

$$OF = \min_{f_s,\,\Delta t_s,\,\Delta dl_s}\left\{\sum_{sc}\left(\pi^{sc}\sum_{s}\Delta dl_s\right)\right\} \tag{11}$$

This is if the frequency curve $\Delta f_n^{sc,h}$ violates the frequency f_0 for a period longer than Δt_s^h. To model the relay timer, a set of equations and inequalities is presented in Eqs. (12)–(15). Here, the binary variables $X_{s,n}^{sc,h}$ defines a timer for the set-point frequency f_s^h as Eqs. (12) and (13).

Hence, with respect to $X_{s,n}^{sc,h}$, the total time that the frequency curve falls below the set-point frequency f_s^h, at scenario sc and hour h has been characterized under Eq. (14). Eq. (15) explains that if the system frequency is higher than set-point f_s^h, the relay timer is reset.

$$\frac{f_s^h - (f_0 + \Delta f_n^{sc,h})}{L_1} \leqslant X_{s,n}^{sc,h} \leqslant 1 + \frac{f_s^h - (f_0 + \Delta f_n^{sc,h})}{L_1}, \quad L_1 \gg 0 \tag{12}$$

$$X_{s,n}^{sc,h} = \begin{cases} 0 & f_0 + \Delta f_n^{sc,h} > f_s^h \\ 1 & f_0 + \Delta f_n^{sc,h} < f_s^h \end{cases} \tag{13}$$

$$\Delta t_{s,n}^{sc,h} = \Delta t_{s,n-1}^{sc,h} + X_{s,n}^{sc,h}\Delta t \tag{14}$$

$$\Delta t_{s.,n}^{sc,h} = N \times X_{s,n}^{sc,h} \qquad \forall\, N \geqslant n \tag{15}$$

In Eqs. (16)–(22), the mathematical model of the relay operating logic is expressed. The relay operating logic addresses that whenever the system frequency falls below f_s^h and $\Delta t_{s,n}^{sc,h} > \Delta t_s$, the load Δdl_s^h is sheds. Therefore, the relay operating logic is modeled by the binary variable of load shedding $Y_{s,n}^{sc,h}$ according to Eq. (16). Here, constraint Eq. (17) should be taken in to account for a binary variable $Y_{s,n}^{sc,h}$. Also, according to Eq. (18), Δt_s^h should be greater than the minimum time required to activate the circuit breaker. Eq. (19) explains that if the load block Δdl_s^h is shed at hour h and stage s, it should not be restored at a later time. Besides, conditions should be considered that the stages of load shedding must not be simultaneous according to Eq. (20). Eventually, as shown in Eq. (21), higher priority loads must be eliminated as far as possible in the last stage. Then, Eq. (7), must be rewritten at scenario sc, hour h and time step n under Eq. (22).

$$\frac{(\Delta t_{s,n}^{sc,h} - \Delta t_s^h)}{L_2} \leqslant Y_{s,n}^{sc,h} \leqslant 1 + \frac{(\Delta t_{s,n}^{sc,h} - \Delta t_s^h)}{L_2}, \quad L_2 \gg 0 \tag{16}$$

$$Y_{s,n}^{sc,h} = \begin{cases} 0 & \Delta t_n^{sc,h} < \Delta t_s^h \\ 1 & \Delta t_n^{sc,h} > \Delta t_s^h \end{cases} \tag{17}$$

$$\Delta t_s^h \geqslant \Delta t_{min} \tag{18}$$

$$Y_{s,n}^{sc,h} \geqslant Y_{s,n-1}^{sc,h} \tag{19}$$

$$\sum_s Y_{s,n}^{sc,h} - \sum_s Y_{s,n-1}^{sc,h} \leqslant 1 \tag{20}$$

$$Y_{s,n}^{sc,h} \geqslant Y_{s+1,n}^{sc,h} \tag{21}$$

$$\Delta f_n^{sc,h} = \Delta f_{n-1}^{sc,h} + RCF_{n-1}^{sc,h}\Delta t \tag{22}$$

In a successful load shedding strategy, the frequency must be within the under-frequency/time range of the manufacturer to ensure that the system generators do not get damaged whenever the frequency falls below a certain threshold. Therefore, there is the number of n_b frequency threshold of manufacturer f_b for the maximum allowed times of the frequency drop Δt_b^{max}. For this purpose, according to Eqs. (23) and (24), this constraint is expressed in the adaptive setting of relay parameters, by introducing the binary variable $Z_{b,n}^{sc,h}$. Hence, the sum of time spent by the system frequency below a specified set-point has been achieved as Eq. (25). To consider the under-frequency/time limitations of the manufacturer, the constraint Eq. (26) must be taken into account in the under-frequency relay setting.

$$\frac{f_b - (f_0 + \Delta f_n^{sc,h})}{L_3} \leqslant Z_{c,n}^{sc,h} \leqslant 1 + \frac{f_b - (f_0 + \Delta f_n^{sc,h})}{L_3}, \quad L_3 \gg 0 \tag{23}$$

$$Z_{b,n}^{sc,h} = \begin{cases} 0 & f_0 + \Delta f_n^{sc,h} > f_b \\ 1 & f_0 + \Delta f_n^{sc,h} < f_b \end{cases} \tag{24}$$

$$\Delta t_{b,n}^{sc,h} = \Delta t_{b,n-1}^{sc,h} + Z_{b,n}^{sc,h}\Delta t \tag{25}$$

$$\Delta t_{b,n}^{sc,h} \leqslant \Delta t_b^{max} \tag{26}$$

It should be noted that the frequency deviation in the last step N after the load shedding must fall within the safe range in Eqs. (27) and (28).

$$-0.5\text{Hz} \leqslant \Delta f_N^{sc,h} \leqslant 0.5\text{Hz} \tag{27}$$

$$\Delta f_N^{sc,h} = \left(\frac{-\Delta G^{sc,h} + \sum_s U_{s,N}^{sc,h}}{D + \frac{1}{R^{sc,h}}} \right) \tag{28}$$

To minimize the frequency oscillation near the steady-state, these oscillations in the last time steps n_{lt} must be within the range shown in Eq. (29). To prevent the early load shedding, Eq. (30) must be also determined for the frequency set-point.

$$-0.15\text{Hz} \leqslant \Delta f_N^{sc,h} - \frac{1}{n_{lt}} \sum_{N-n_{lt}} \Delta f_n^{sc,h} \leqslant 0.15\text{Hz} \tag{29}$$

$$\min_b(f_b) \leqslant f_s^h \leqslant max(f) \tag{30}$$

Eventually, the constraint of Eq. (31) must be considered so that the frequencies of the consecutive steps of load shedding are not equal.

$$0.1Hz \leqslant f_s^h - f_{s+1}^h \tag{31}$$

With respect to the ever-increasing penetration of RES in the smart grid, variations in wind and solar power generation and load fluctuations affect the frequency of the system. Finally, the effect of these uncertainties and DR on the adaptive setting of the under-frequency relay should be considered. In this paper, according to Eq. (32), the DR program is introduced as a straight line that decreases and is assumed to lie between the upper D_{max} and lower D_{min} limits.

$$D_{min} \leqslant Pdr \leqslant D_{max} \tag{32}$$

Therefore, in Eq. (8), the factors of wind generation, $\Delta P_w^{sc,h}$, solar generation, $\Delta P_{pv}^{sc,h}$, load fluctuations, $\Delta P_{lf}^{sc,h}$ and DR, $Pdr^{sc,h}$ are added and then Eq. (33) is obtained as the final model for the proposed adaptive UFLS strategy.

$$\begin{aligned} RCF_n^{sc,h} &= \frac{f_0}{2H^{sc,h}}(\Delta R_n^{sc,h} - \Delta G^{sc,h} - D\Delta f_n^{sc,h} - \Delta P_w^{sc,h} - \Delta P_{pv}^{sc,h} - \Delta P_{lf}^{sc,h} \\ &\quad + Pdr^{sc,h} + \sum_s \Delta dl_s^h) \end{aligned} \tag{33}$$

The model of the system frequency response is expressed by Laplace transform as Eqs. (34) and (35):

$$\begin{aligned} \Delta f(s) &= \frac{f_0}{2Hs}(\Delta R(s) - \Delta G(s) - D\Delta f(s) - \Delta P_w(s) - \Delta P_{pv}(s) - \Delta P_{lf}(s) \\ &\quad + Pdr(s) + \sum_s \Delta dl) \end{aligned} \tag{34}$$

$$\Delta R(s) = \frac{-1}{R(1 + Ts)} \Delta f(s) \tag{35}$$

In Fig. 4, The model of the system frequency response is shown as the final model considering the proposed adaptive UFLS scheme. Also, the ELNS index is presented as the expected load not served for evaluating the system security and reliability following Eq. (36). Here, the lower the ELNS index, the greater the system reliability and security [29].

$$ELNS = \sum_{sc} \sum_s \sum_h \pi^{sc} \Delta dl_s^h \tag{36}$$

3. Simulation results

In the present paper, the proposed adaptive UFLS scheme has been implemented on the IEEE 39-bus test system with 10 generators, 19 loads, 3 wind farms, 2 solar farms, and 2 demand responses over a 24-hour time horizon. The input parameters of the system and the nominal values of the generators are indicated in Tables 1 and 2, respectively. All the values are based on 100 MVA. All the simulations have been implemented at 200 time steps.

Fig. 5 illustrates the proposed adaptive UFLS strategy based on the MILP formulation. In this figure, the system information is extracted at each hour. Then, hourly scenarios are generated using this information in real-time. These scenarios are applied as input to the MILP optimization process, and the relay parameters are obtained based on the system conditions. According to the relationships mentioned in the previous section, the operation logic, timer, and discrete-time frequency response of the relay are modeled given the operational constraints in the MILP formulation framework. Finally, the under-frequency relay sheds the minimum load at each hour of a day ahead using the obtained parameters. A similar process can be implemented for the following days.

3.1. The proposed adaptive UFLS technique

For the implementation of the proposed adaptive UFLS strategy and achievement of the minimum load shedding, 1000 different scenarios are generated based on the MCS and RWM processes. These scenarios consider uncertainties corresponding to the generation deficiency resulting from contingency, the variations in the solar and wind powers, the load fluctuations, and the presence of DR. Then, the remaining 144 most probable scenarios are used for 24-hour a day ahead, 6 scenarios an hour, based on the scenario reduction algorithm. Below, the simulation results of the proposed method are examined.

In Fig. 6, the frequency waveforms are illustrated in both states with and without relay activity. Here, the value of steady-state frequency is 59.51 Hz with the relay activity, while this value is reduced to 58.32 Hz without the relay activity. Therefore, the relay successfully restores the system frequency to a safe range. Two cases have been studied here for the simulation of the proposed method, following Table 3. In case 1, all the uncertainties concerning variations in RES power, load fluctuations, and generation deficiency have been investigated. In case 2, the effect of DR in the setting of the under-frequency relay parameters has been evaluated along with the consideration of the above uncertainties.

Fig. 7 shows the simulation results for the 24-hour setting of the relay parameters in case 1. It illustrates the 24 parameter sets that were collected to adjust the under-frequency relays. Each of these sets of parameters corresponds to a specific hour, obtained according to the system conditions at that hour. At hours when the intensity of the

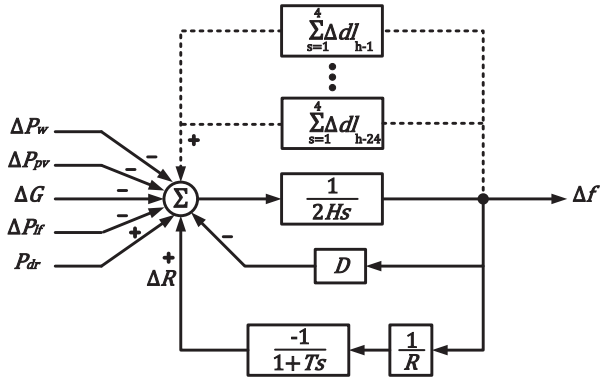

Fig. 4. Model of system frequency response for the proposed adaptive UFLS scheme.

Table 1
Input parameters for the IEEE 39-bus test system [30].

Nominal frequency of the system, f_n, (Hz)	60
The time constant of the equivalent inertia, H, (s)	4
Load Damping, D, (pu)	2
governor equivalent droop, R, (%)	5
Minimum Frequency Difference Between consecutive Stages of Load Shedding, $\Delta f_{\min}$, (Hz)	0.1

disturbance and contingency are mild, frequency drop is less, and less load is therefore shed. Conversely, at hours of peak load, the amount of load that is shed increases significantly as a result of the imbalance between load and generation. In case 1, load shedding has increased at each hour due to the destructive effect of the presence of RESs and instantaneous load fluctuations on system frequency. This results from the uncertain nature of these sources. The presence of RESs and load fluctuations in the power system increases the frequency oscillations and endangers the stability of the system. Therefore, the under-frequency relay must shed a large amount of load to prevent system frequency collapse. Therefore, average load shedding has reached 0.419pu. In this case, different set-point frequencies have been obtained at each hour, and the set-point frequency at each stage increases as the amount of load shedding decreases. This is because frequency deviation is reduced, and the excessive load is therefore shed at a higher frequency. The delay time at each of the four stages is 0.2 s.

In case 2, the effect of DR on system frequency and the amount of load that is shed is investigated as well as the conditions stated for case 1. Fig. 8 presents the results of the adaptive UFLS strategy in case 2 at each hour of a day ahead. A comparison of Figs. 7 and 8 demonstrates that at hours when the RES outputs and load fluctuations increase in case 2, and the uncertainties have great effects on system frequency, DR reduces the load shed at each hour with respect to that in case 1 (particularly at peak load) by improving the system frequency response and reducing frequency drop. It should be noted that with the fast telecommunications system and the powerful AMI in the smart grid, the speed of response to the frequency oscillations is high, and the performance of the adaptive UFLS system is appropriate. As shown in Fig. 8, the proposed adaptive UFLS method sheds less average load than in case 1, which is 0.409. Therefore, the destructive effects of RESs and load fluctuations on frequency are reduced in the presence of DR. In this case, delay time is a constant value of 0.2 s, as in the previous case. It is clear that the set-point frequency at each of the four load shedding stages is higher in case 2 than in case 1 due to the presence of DR, which enhances frequency stability. Therefore, DR can have a positive effect on the UFLS process, as a result of which, system reliability and security are increased.

Figs. 9 and 10 illustrate the frequency waveforms over a 24-hour time horizon with the proposed adaptive UFLS system in cases 1 and 2, respectively. According to these figures, the frequency deviation in case 2 is less than that in case 1, and the minimum steady-state frequency in the 24-hour period is 59.503 Hz in case 1, which is increased to 59.586 Hz in case 2, resulting from the positive effect of DR on system frequency. Therefore, DR is successful here in the improvement of the frequency response of the system, and it thus reduces the amount of load shedding. Hence, the proposed adaptive UFLS system successfully returns system frequency to the safe range at all hours, while preventing system frequency collapse. In case 2, the initial deviation of frequency has been reduced significantly with respect to that in case 1.

Figs. 11 and 12 show the ROCOF values over a 24-hour time horizon in cases 1 and 2, respectively. In these figures, the bar graphs show the ROCOF value at each hour for scenarios 1 to 6, and each segment of the bar graphs represents one scenario. Here, the ROCOF value varies by the hour conditions and the intensity of contingency. In case 2, the ROCOF value is significantly lower than that in case 1 due to the presence of DR and the decrease in frequency deviations. Thus, DR decreases the ROCOF value in each scenario by increasing the equivalent inertia constant of the system, decreasing the amount of load that is shed. Figs. 13 and 14 depict the $|f_0 - f_{nadir}|$ value at each hour for six scenarios in cases 1 and 2, respectively. Here, f_{nadir} is the minimum frequency created by a disturbance in the system. In case 2, $|f_0 - f_{nadir}|$ has decreased with respect to that in case 1 with the presence of DR. In Fig. 15, the proposed adaptive UFLS strategy is illustrated at four stages for cases 1 and 2. Here, f_{nadir} is greater in case 2 than in case 1, as stated above. Moreover, the frequency set-point of each load shedding stage in case 2 has increased with respect to that in case 1. The gradient of each stage represents the ROCOF value. Based on the results obtained from the simulations, the values of the ELNS index in cases 1 and 2 are 19.032 and 17.349, respectively. Hence, the ELNS value in case 2 has been reduced with respect to that in case 1 due to the presence of DR, and the security and reliability of the system have therefore been enhanced in case 2.

3.2. Discussion and comparison

In this section, it is assumed that the relay parameters are not hourly set, and the same setting is given at all hours. Hence, the most probable scenarios, including the mildest, medium, and most severe, are generated by the process of MCS and RWM and the scenario reduction algorithm. The under-frequency relay parameters are then set using the MILP formulation. In this case, the objective function is written as Eq. (11).

Table 4 shows the simulation results for the UFLS strategy in cases 1 and 2, as in the previous section. In the proposed adaptive UFLS method, the average amount of load shedding during the 24 h of a day ahead is the criterion for comparison. According to the table, the amount of load shed in case 1 has increased by 27% with respect to a similar case in the adaptive UFLS strategy, reaching a value of 0.533pu. The amount of excessive load shed in case 2 has also increased by 21%. In this case, the amount of 0.498pu has been shed from the load. It is also observed that the frequency set-point value has been reduced with respect to that in the adaptive UFLS method, and the risk of system frequency collapse is therefore lower in the adaptive UFLS method than in the non-hourly method. The time delay value in both methods is 0.2 s.

Therefore, the UFLS is performed more accurately in the adaptive UFLS strategy due to the specific conditions at each hour, examined by the advanced measurement devices in the smart grid. The smaller the time interval in the setting of the relay parameters (for example, a fifteen-minute rather than one-hour interval), the lower the amount of load shedding. Program execution time is greatly increased, however, which reduces the efficiency of the proposed method.

4. Conclusion

In this paper, an adaptive UFLS scheme has been proposed to be applied in smart grids. In the relevant strategy, the load shedding process is based on the precise mathematical formulation in real-time. The under-frequency relay parameters including set-point frequency,

Table 2
Nominal output of the system generators (pu) [30].

Gen1	Gen2	Gen3	Gen4	Gen5	Gen6	Gen7	Gen8	Gen9	Gen10
0.1588	0.1076	0.1032	0.1003	0.0806	0.1032	0.0890	0.0857	0.1318	0.0398

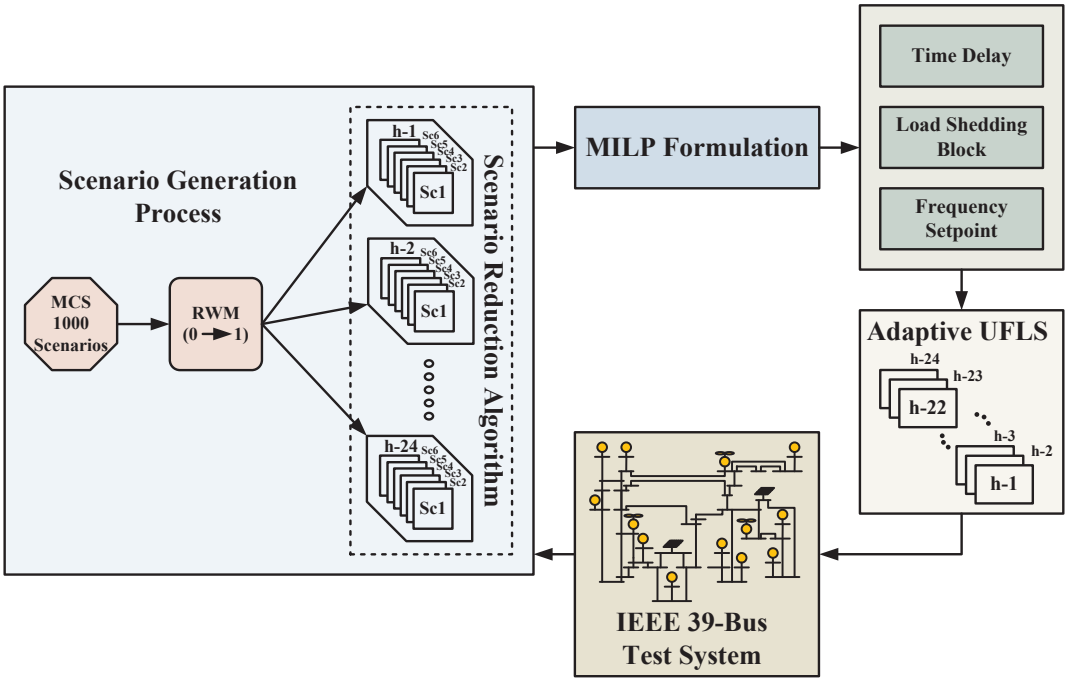

Fig. 5. Block diagram of the proposed adaptive UFLS scheme.

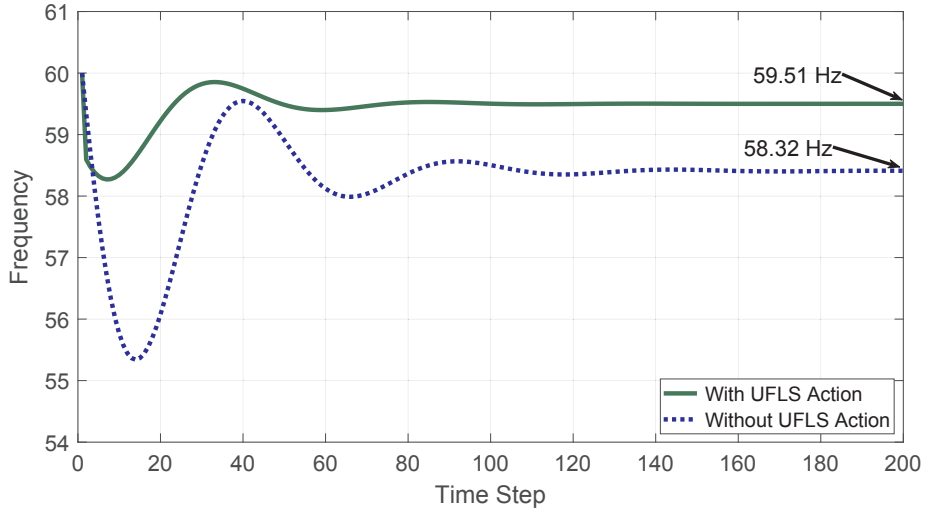

Fig. 6. Contingency of generation deficiency with and without UFLS action.

Table 3
Characteristics of cases 1 and 2.

Case No.	Uncertainty Resources			DR
	Generation Deficiency	RES	Load Fluctuations	
Case 1	✓	✓	✓	✗
Case 2	✓	✓	✓	✓

time delay, and load shedding block have been set at each hour of a day ahead. Therefore, six different scenarios at each hour have been generated by the MCS, RWM, and scenario reduction algorithm processes. These scenarios have been applied to the IEEE 39-bus test system. Then, the objective function has been optimized over a 24-hour time horizon given all the conditions in the MILP formulation. According to the results, the DR improves the system frequency response and eliminates the adverse effects of RES power and load fluctuations as system inertia capacity increases. Finally, the results of the proposed strategy have been compared to those for the non-hourly UFLS scheme. The proposed method is highly adaptable in different operating conditions of the power system. Given the high accuracy of the proposed strategy, it can reduce the problems associated with conventional load shedding methods and improve the stability of the power system. The key findings of this paper are summarized below.

- Smart grid technologies can be used to enhance the efficiency of UFLS protection schemes.
- Since the exact mathematical model of the under-frequency relay has been obtained, the results of the simulations are close to reality.
- The positive effect of DR on the frequency response of the system as well as on the reduction of load shedding has been demonstrated.
- The integration of DR, RES, load fluctuation and adaptive UFLS in the smart grid has enhanced system reliability, security, and sustainability.

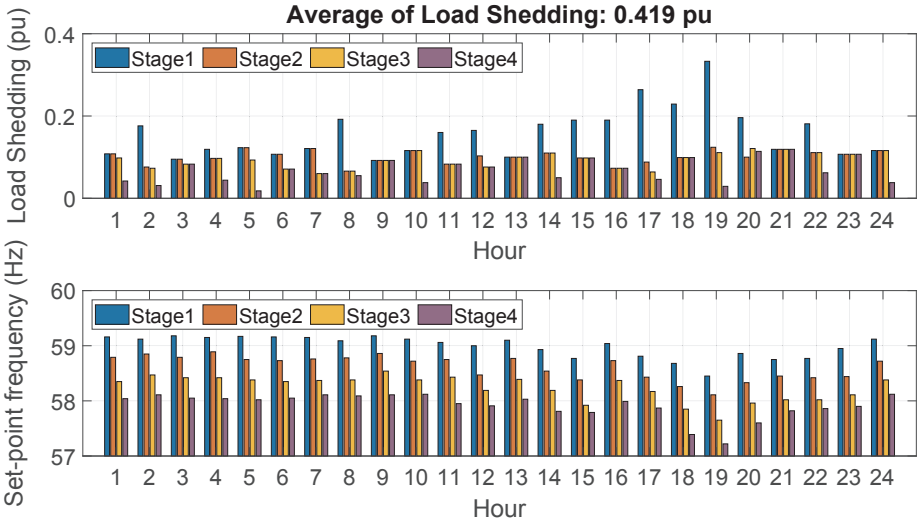

Fig. 7. Simulation results in case 1 to evaluate the adaptive UFLS proposed scheme.

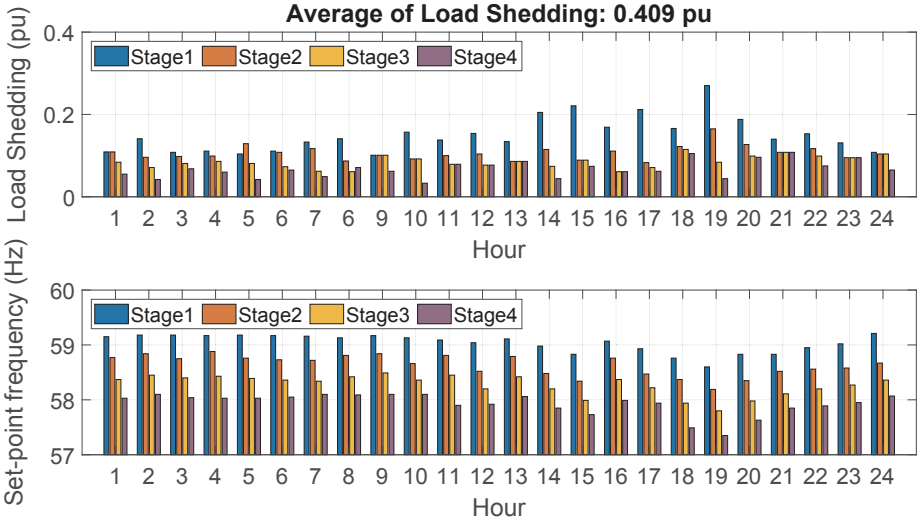

Fig. 8. Simulation results in case 2 to evaluate the adaptive UFLS proposed scheme.

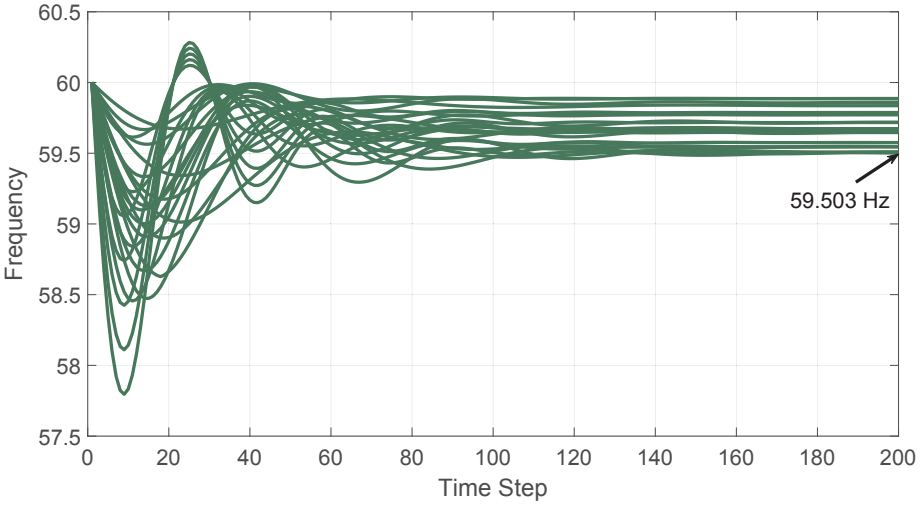

Fig. 9. System frequency waveform over a 24-hour time horizon in cases 1.

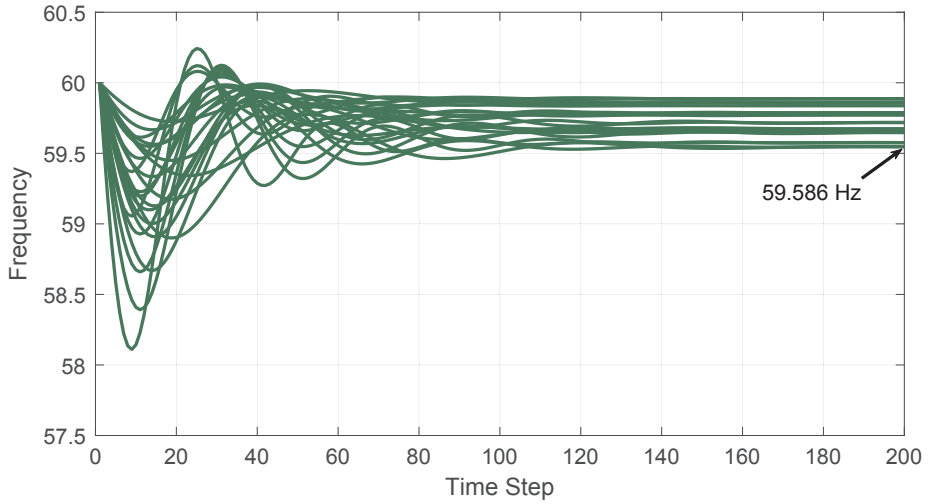

Fig. 10. System frequency waveform over a 24-hour time horizon in cases 2.

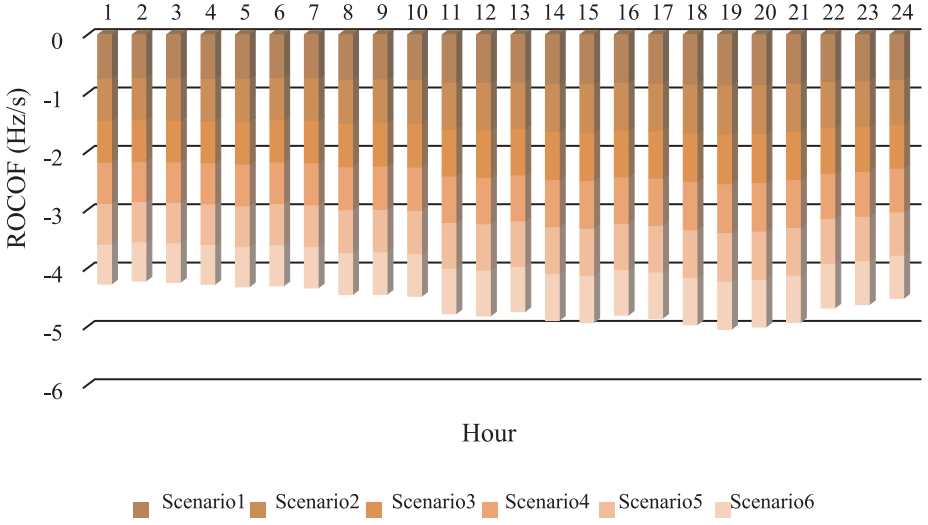

Fig. 11. Changes in the ROCOF value from hour-1 to hour-24 in case 1.

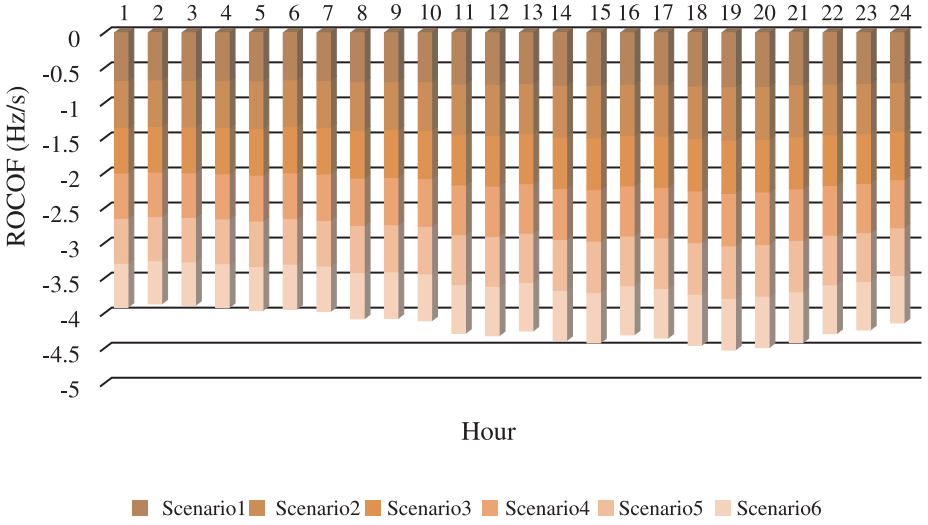

Fig. 12. Changes in the ROCOF value from hour-1 to hour-24 in case 2.

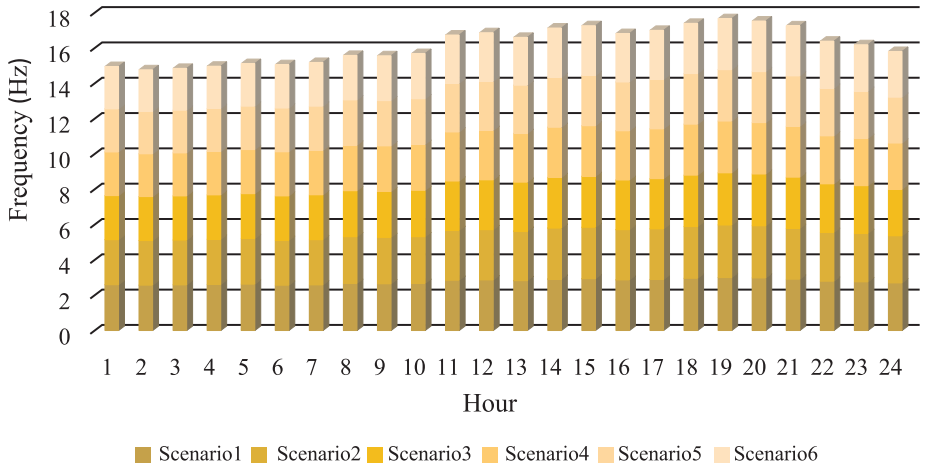

Fig. 13. Changes in the $|f_0 - f_{nadir}|$ value from hour-1 to hour-24 in case 1.

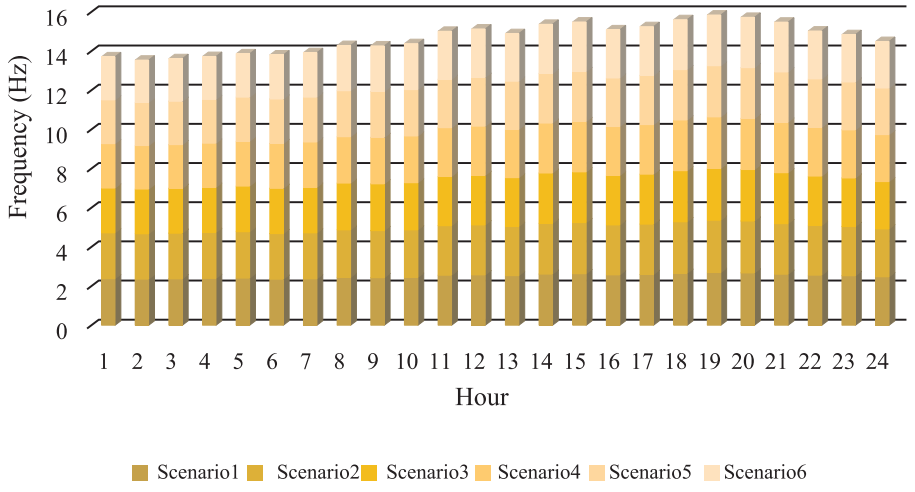

Fig. 14. Changes in the $|f_0 - f_{nadir}|$ value from hour-1 to hour-24 in case 2.

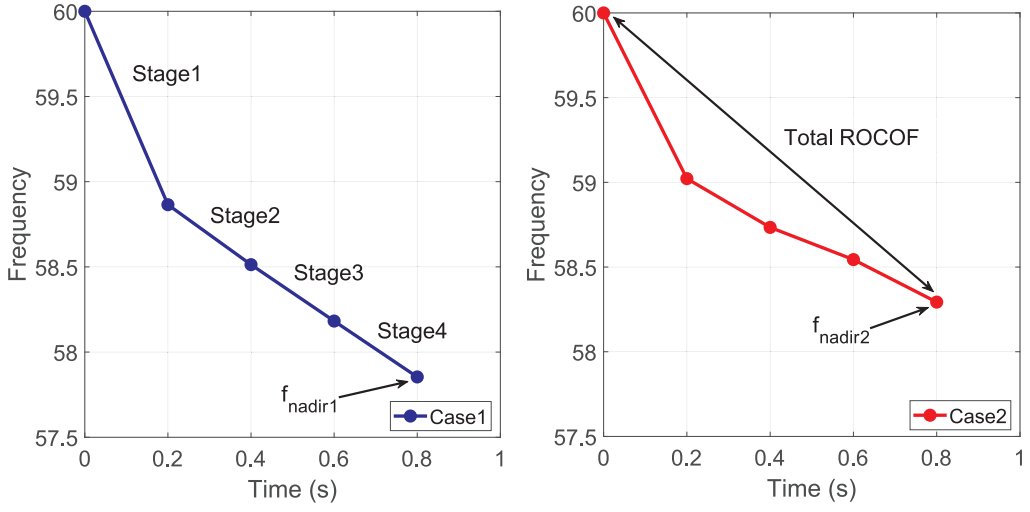

Fig. 15. Different stages of load shedding in cases 1 and 2.

CRediT authorship contribution statement

Ali Rafinia: Conceptualization, Data curation, Formal analysis, Funding acquisition, Writing - original draft, Writing - review & editing. **Navid Rezaei:** Investigation, Methodology, Resources, Software, Supervision. **Jamal Moshtagh:** Validation, Visualization, Project administration.

Table 4
Simulation results for non-hourly UFLS strategy in cases 1 and 2.

Parameter	Set-point frequency, f_s^h, Hz				Time delay, $\Delta\ t_s^h$, s				Load shedding block, Δdl_s^h, pu				
	St-1	St-2	St-3	St-4	St-1	St-2	St-3	St-4	St-1	St-2	St-3	St-4	Total
Case 1	58.86	58.51	58.18	57.85	0.2	0.2	0.2	0.2	0.114	0.170	0.149	0.100	0.533
Case 2	58.99	58.75	58.55	58.01	0.2	0.2	0.2	0.2	0.176	0.076	0.073	0.031	0.498

Declaration of Competing Interest

The authors declared that there is no conflict of interest.

References

[1] Laghari JA, Mokhlis H, Karimi M, Bakar AHA, Mohamad H. A new under-frequency load shedding technique based on combination of fixed and random priority of loads for smart grid applications. IEEE Trans Power Syst 2015;30:2507–15.
[2] Tabandeh A, Abdollahi A, Rashidinejad M. Reliability constrained congestion management with uncertain negawatt demand response firms considering repairable advanced metering infrastructures. Energy 2016;104:213–28.
[3] Rudez U, Mihalic R. WAMS-based underfrequency load shedding with short-term frequency prediction. IEEE Trans Power Delivery 2016;31:1912–20.
[4] Rudez U, Mihalic R. Monitoring the first frequency derivative to improve adaptive underfrequency load-shedding schemes. IEEE Trans Power Syst 2011;26:839–46.
[5] Abdelwahid S, Babiker A, Eltom A, Kobet G. Hardware implementation of an automatic adaptive centralized underfrequency load shedding scheme. IEEE Trans Power Delivery 2014;29:2664–73.
[6] Xia N, Gooi HB, Abur A, Chen SX, Eddy YSF, Hu W. Enhanced state estimator incorporating adaptive underfrequency load shedding under contingencies via the alternating optimization method. Electr Power Energy Syst 2016;81:239–47.
[7] Santos AQ, Monaro RM, Coury DW, Oleskovicz M. A new real-time multi-agent system for under frequency load shedding in a smart grid context. Electr Power Syst Res 2019;174:105851.
[8] Talaat M, Yatata AY, Alsayyari AS, Alblawi A. A smart load management system based on the grasshopper optimization algorithm using the under-frequency load shedding approach. Energy 2020;190:116423.
[9] Aparicio N, Villalba SA, Belenguer E, Gimenez RB. Automatic under-frequency load shedding mal-operation in power systems with high wind power penetration. Math Comput Simul 2018;146:200–9.
[10] Gu W, Liu W, Zhu J, Zhao B, Wu Z, Luo Z, et al. Adaptive decentralized under-frequency load shedding for islanded smart distribution networks. IEEE Trans Sustain Energy 2014;5:886–95.
[11] Li H, Wang J, Du Z, Zhao F, Liang H, Zhou B. Frequency control framework of power system with high wind penetration considering demand response and energy storage. The 6th international conference on renewable power generation. 2017. p. 19–20.
[12] He P, Wen B, Wang H. Decentralized adaptive under frequency load shedding scheme based on load information. IEEE Access 2019;7:52007–14.
[13] Banijamali SS, Amraee T. Semi-adaptive setting of under frequency load shedding relays considering credible generation outage scenarios. IEEE Trans Power Delivery 2019;34:1098–108.
[14] Shekari T, Gholami A, Aminifar F. Sanaye-Pasand. An adaptive wide-area load shedding scheme incorporating power system real-time limitations. IEEE Syst J 2018;12:759–67.
[15] Atighechi H, Hu P, Ebrahimi S, Lu J, Wang G, Wang L. An effective load shedding remedial action scheme considering wind farms generation. Int J Electr Power Energy Syst 2018;95:353–63.
[16] Amraee T, Darenaghi MG, Soroudi A, Keane A. Probabilistic under frequency load shedding considering RoCoF relays of distributed generators. IEEE Trans Power Syst 2018;33:3587–98.
[17] Darebaghi MG, Amraee A. Dynamic multistage under frequency load shedding considering uncertainty of generation loss. IET Generat, Trans, Distribut 2017;11:3202–9.
[18] Zhenglong S, Guowei C, Yuwei W, Jiarong S. A method for the design of UFLS schemes of regional power system using improved frequency response model. Int Trans Electr Energy Syst 2017;2365:1–11.
[19] Ketabi A, Fini MH. Adaptive under frequency load shedding using particle swarm optimization algorithm. J Appl Res Technol 2017;15:54–60.
[20] Gomez C, Qadri SS, Galiana F. Under-frequency load shedding via integer programming. IEEE Trans Power Syst 2012;27:1387–94.
[21] Alagoz BB, Kaygusuz A, Akcin M, Alagoz S. A closed-loop energy price controlling method for real-time energy balancing in a smart grid energy market. Energy 2013;59:95–104.
[22] Alagoz BB, Kaygusuz A. Dynamic energy pricing by closed-loop fractional-order PI control system and energy balancing in smart grid energy markets. Trans Inst Meas Control 2016;38:565–78.
[23] Mak ST, So E. Integration of PMU, SCADA, AMI to accomplish expanded functional capabilities of Smart Grid. 29th conference on precision electromagnetic measurements August 2014:1–2.
[24] Rudez U, Mihalic R. Predictive underfrequency load shedding scheme for islanded power systems with renewable generation. Electr Power Syst Res 2015;126:21–8.
[25] Rezaei N, Kalantar M. Stochastic frequency-security constrained energy and reserve management of an inverter interfaced islanded microgrid considering demand response programs. Int J Electr Power Energy Syst 2015;69:273–86.
[26] Rezaei N, Kalantar M. Hierarchical energy and frequency security pricing in a smart microgrid: An equilibrium inspired epsilon constraint based multi-objective decision making approach. Energy Convers Manage 2015;98:533–43.
[27] Rezaei N, Kalantar M. Smart microgrid hierarchical frequency control ancillary service provision based on virtual inertia concept: An integrated demand response and droop controlled distributed generation framework. Energy Convers Manage 2015;92:287–301.
[28] Kundur P, Balu N, Lauby M. Power system stability and control. 7th ed. New York: McGraw-Hill Inc; 1994.
[29] Rezaei N, Kalantar M. Economic–environmental hierarchical frequency management of a droop-controlled islanded microgrid. Energy Convers Manage 2014;88:498–515.
[30] Pai A. Energy function analysis for power system stability. Springer Science & Business. Media 2012.